Experimental study of nonlinear beam dynamics at VEPP-4M

V. Kiselev, E. Levichev, V. Sajaev*, V. Smaluk

Budker Institute of Nuclear Physics, Novosibirsk 630090, Russia

Received 15 October 1997

Abstract

Nonlinear dynamics of transverse beam motion has been studied experimentally at the VEPP-4M electron–positron collider. Two aspects of nonlinear beam behaviour described in this paper are the amplitude-dependent tune shift and the phase space trajectories near nonlinear resonances. The measurement results are presented and compared with the theoretical prediction. © 1998 Elsevier Science B.V. All rights reserved.

1. Introduction

Despite the progress in explanation of nonlinear phenomena in circular accelerators, there still is a gap between computer simulations or analytical predictions and reality. To reduce this gap, many dedicated experiments have been performed in both hadron and lepton machines in recent years. The list, far from being complete, includes dynamic aperture experiment at the Indiana University Cyclotron Facility [1,2], various measurements in the vicinity of the $\frac{2}{5}$ resonance in the Fermilab E778 experiment [3,4], the third-resonance study at the Aladdin electron ring, Wisconsin [5,6], nonlinear dynamics study at TRISTAN [7], etc. More complete and well-prepared report can be found in Refs. [8,9].

As it was recently found [10], the dynamic aperture of VEPP-4M is strongly affected by magnetic

field nonlinearities. The measured value of the dynamic aperture does not follow the lattice model with nonlinear components computed from direct magnetic measurements. In order to explain this discrepancy and establish possible sources of nonlinearities, phase space features were measured extensively at the VEPP-4M storage ring in 1995–1996.

This paper concerns the study of phase space topology and nonlinear detuning under various experimental conditions (betatron tunes, sextupoles and octupoles strength, etc.). Motion of the gravity centre of the beam was measured turn by turn after excitation of coherent betatron oscillations by a fast kicker magnet. Two ways of phase map plotting were examined: by two BPM stations and by a single BPM. FFT, when applied to the coordinate array, provides a significant noise reduction and an increase of trajectory resolution. The amplitude-dependent tune shift was studied for both sextupole and octupole perturbation. The experimental data agree quite well with the tracking simulation and model prediction.

*Corresponding author. Tel.: +7 3832 359289; fax: +7 3832 352163; e-mail: sajaev@inp.nsk.su.

2. Hardware description

The VEPP-4M storage ring is a 6 GeV electron–positron collider with a circumference of 366 m. The study was performed at an injection energy of 1.8 GeV. The relevant parameters of VEPP-4M at this energy are given in Table 1.

To produce coherent transverse motion, the beam is kicked vertically or horizontally by pulsed electromagnetic kickers. The pulse duration is 50 ns for the horizontal kicker and 150 ns for the vertical one. Oscillation of the beam centroid and beam intensity are measured turn by turn with a beam position monitor (BPM) SRP3 for up to 4096 revolutions. The rms displacement resolution is $\sigma_{x,z} \simeq$ 70 μm in a 1–5 mA beam current range.

For a theoretical prediction the following sources of magnetic field nonlinearity were taken into account:

1. 32 vertical and horizontal sextupole corrections distributed along the magnets in the arcs (two families, DS and FS).
2. Lumped sextupoles SES2, NES2 and SES3, NES3 located symmetrically around the interaction point.
3. Quadratic field component produced by the arc magnet pole shape (two families, SSF and SSD).
4. Octupole correction coils incorporated in the arc magnet main coils (32 corrections, two families, SRO and NRO).

Main parameters of the nonlinear elements mentioned above are listed in Table 2.

Because of high beta-function values ($\simeq 120$ m), a bulk of natural chromaticity of the ring is produced by the final focus quadrupoles ($\simeq 50\%$ in a horizontal plane and $\simeq 60\%$ in a vertical plane).

Table 1
Beam parameters for the experiment

Energy	1.8 GeV
Revolution period	1.2 μs
Betatron tunes (h/v)	8.620/7.560
Natural chromaticity (h/v)	− 13.6/ − 20.7
Horizontal emittance	35 nm rad
Rms beam bunch length	6 cm
Damping times (h/v/long.)	35/70/70 ms

Table 2
Main parameters of the nonlinear elements

Name	No	Length (m)	d^2B/dx^2 (T/m²)
SSD	32	1.114	− 1.68
SSF	32	1.113	1.11
SES2/NES2	4	0.20	9.25
SES3/NES3	2	0.20	− 16.25
FS	32	0.342	5.24
DS	32	0.342	− 9.25

This chromaticity is locally compensated by the SES2/NES2 and SES3/NES3 sextupoles. Hence, we can expect that the influence of these sextupoles on the nonlinear dynamics should be emphasized.

3. Amplitude-dependent tune shift

Coherent beam oscillation is fired by several kicker pulses with different amplitudes, and tune was extracted from a FFT spectrum of 1024 revolutions. To avoid decoherence and various damping mechanisms, a special algorithm is developed to extract beam displacement from first 30–50 revolutions. The accuracy of the tune measurement is better than 2×10^{-4}. Before kick measurement the following preparatory adjustments and calibrations are made:

1. Beta-functions are carefully measured in the SRP3 pickup station ($\beta_z = 12$ m, $\beta_x = 4$ m) and compared with those obtained by the model calculation ($\beta_z = 13.2$ m, $\beta_x = 4.5$ m).
2. Tune-current dependence is measured ($\delta v_x = -3 \times 10^{-4}$ mA^{-1}, $\delta v_z = -1.3 \times 10^{-3}$ mA^{-1}) and taken into account while studying the nonlinear detuning. To reduce this effect, in every kick series the beam intensity is dropped down for less than 0.3 mA.
3. The linearity and absolute kick amplitude calibration is made by scrapers with an accuracy better than 0.1 mm.
4. The betatron tunes are set to the desirable point by quadrupole lenses, the closed orbit distortion is corrected and the chromaticity is adjusted to ≈ 1.

For the Hamiltonian composed of a nonperturbed part H_0 and a small perturbation H_1

$$H(J, \phi, \theta) = H_0(J) + H_1(J, \phi, \theta), \tag{1}$$

where the perturbation itself consists of constant and oscillated parts

$$H_1(J, \phi, \theta) = \bar{H}_1(J) + \tilde{H}_1(J, \phi, \theta),$$

the amplitude-dependent tune shift is defined as

$$\Delta v(J) = \mathrm{d}\bar{H}_1(J)/\mathrm{d}J.$$

For both octupole and sextupole perturbation, the nonlinear tune shift is proportional to the squared initial beam displacement (Fig. 1). A general 2D form of the amplitude-dependent tune shift can be expressed as (a second-order approximation):

$$\Delta v_x(a_x, a_z) = C_{11} \cdot 2J_x + C_{12} \cdot 2J_z,$$

$$\Delta v_z(a_x, a_z) = C_{21} \cdot 2J_x + C_{22} \cdot 2J_z,$$

where C_{nm} depends on particular perturbative potential. The measured and estimated coefficient values are listed in Table 3.

The difference in theoretical and experimental C_{11} made us explore systematically the horizontal

Table 3
Nonlinear detuning coefficients

$C_{nm} \times 10^4$ (m^{-1})	Theory	Experiment
C_{11}	44	3900
C_{12}	-840	-1400
C_{21}	-840	-1750
C_{22}	-830	-1400

nonlinearity of the ring. The later may be induced by octupole and/or sextupole (in second order) errors that we did not consider in our model simulation. To distinguish, which one defines C_{11} in our case, we used the difference between the determination of the octupole and sextupole tune shift. For an octupole potential the horizontal tune shift is independent on an initial tune value [11]

$$\Delta v_x^{(o)}(J_x) = \frac{J_x}{16\pi} \int_0^C O(s)\beta_x^2(s) \,\mathrm{d}s + \mathrm{o}(J_x^2), \tag{2}$$

where C is the machine circumference and $O(s) = (\mathrm{d}^3 B_z(s)/\mathrm{d}x^3)/B\rho$ is the effective octupole strength. Sextupole tune shift on the contrary depends on an
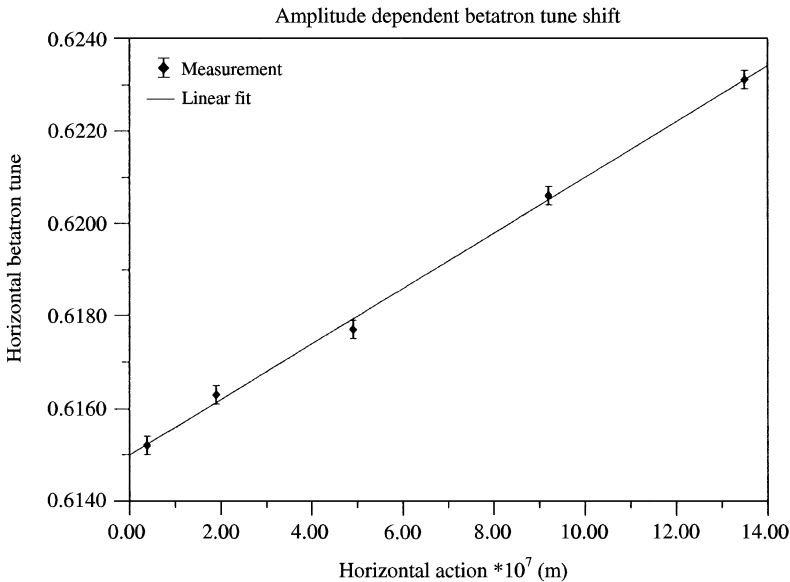

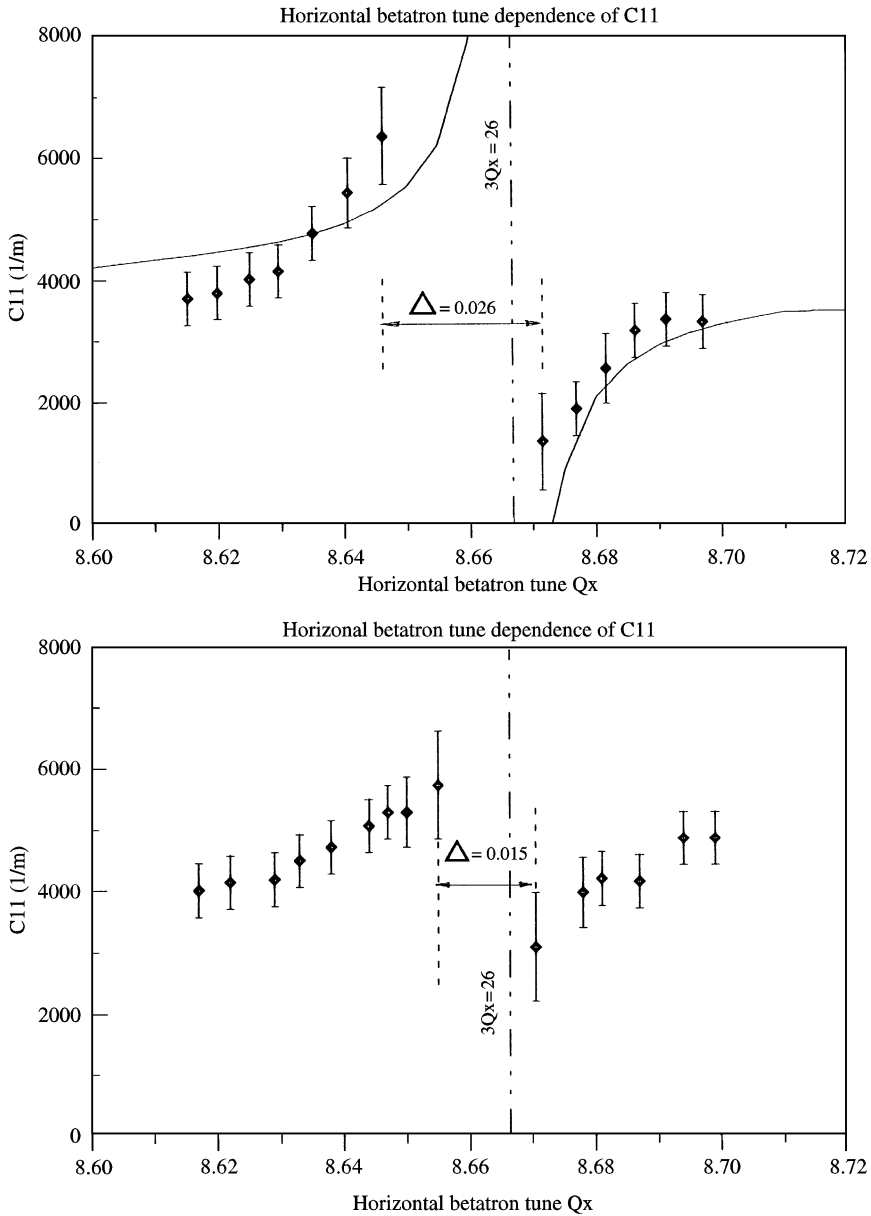Fig. 1. Typical amplitude dependence of the betatron tune.

Fig. 2. C_{11} behaviour near a resonance $3\nu_x = 26$ with normal (top) and reduced (bottom) sextupole driving term. Data points are measured; the curve is predicted.

initial tune near the resonance $3\nu_{x0} \simeq m$ in a reson-ant way and can be written as

$$\Delta\nu_x^{(s)}(J_x) \simeq -J_x \cdot 36 \frac{A_{3m}^2}{3\nu_x - m} + \mathrm{o}(J_x^2),$$

where A_{3m} is the azimuthal harmonic of the sex-tupole Hamiltonian. The measured horizontal tune shift as a function of an initial tune ν_{x0} in the vicinity of the resonance $3\nu_{x0} = 26$ is shown in the top of Fig. 2. To fit the computed curve with the

data points, we should move the curve in positive direction by a value $\Delta v_x^{(o)}/2J_x \simeq 3500\,\text{m}^{-1}$ independently of initial tunes. We can propose that this value is the octupole contribution to the total tune shift.

To verify validity of this assumption, first, we controlled octupole perturbation by the octupole correctors SRO/NRO, distributed along the ring arcs. Changing their excitation current from 0 to $-0.5\,\text{A}$ provides a decrease of the average level of the $C_{11}(v_{x0})$ for all the unperturbed working points v_{x0} to a magnitude $\Delta v_x^{(o)}/2J_x \simeq 1700\,\text{m}^{-1}$, while its resonant behaviour remains the same.

Next, we reduced the sextupole driving term responsible for the resonance $3v_{x0} = 26$. The excitation current of the SES2/NES2 sextupoles was decreased from 8 to 4.4 A and the relevant sextupole harmonic became twice as less. Uncompensated chromaticity was corrected by the sextupole coils in the regular arc magnets. The theory predicts very weak effect of these correctors to the driving term because of a low $\beta_x \simeq 6\,\text{m}$ there. The resulting detuning is shown in the bottom of Fig. 2. One can see that the average level of the detuning retains, while the sextupole contribution is reduced. It is clearly seen from the resonance stopband Δ that was defined as a distance between the points where the beam lifetime became as low as 300–400 s.

A detailed tracking study points out to the final focus (FF) quadrupoles EL1/EL2 as a most probable source of the octupole error. Otherwise we should suppose an unrealistically high nonlinear error in regular arc quadrupoles. It was shown in Ref. [12], that quadrupole edge fields can produce large detuning; however, in our case the relevant contribution to the C_{11} coefficient is ten times as less as the measured one. That is why we suspected that the octupole error was distributed in the FF quadrupoles.

Following this indication, we have done a set of measurements.

1. According to Eq. (2), first we measured quadratic dependence of the octupole detuning on β_x. The excitation current in the quadrupoles EL1/EL2 was changed, the tune point was adjusted back by the arc quadrupole magnets, the chromaticity was compensated and closed orbit distortion was corrected with an accuracy $< 0.2\,\text{mm}$ in the final focus region and $< 0.5\,\text{mm}$ at the rest of the ring. The results of the measurement are presented in Fig. 3 where C_{11} is shown as a function of β_x^2 in the FF quadrupoles. From this result we can estimate the value of the octupole errors as follows:

$$O \simeq 0.5\,\text{G/cm}^3 = 8.1\,\text{m}^{-4}.$$

2. Employing steering coils around the interaction region gives a possibility of measuring integrated magnetic field distribution by an electron beam. We can produce a local symmetric or antisymmetric orbit bump in the horizontal plane as it is shown in Fig. 4, keeping closed orbit distortion in the rest of the ring within 0.5 mm, and measure the betatron tune shift caused by the magnetic nonlinearities. In case of the symmetric bump the main contribution to the tune shift is provided by the chromatic sextupoles SES/NES, located inside the bump and it is difficult to extract the influence of small nonlinear errors in the FF quadrupoles. But in case of the antisymmetric bump the sextupole contribution is substracted and measured betatron tune shift as a function of orbit displacement x in the FF quadrupoles unambiguosly demonstrates presence of integrated octupole nonlinearity (Fig. 5). The orbit deviation in the bump is read by 6 pickup stations and allows one to reconstruct beam displacement in the quadrupoles.

Least-squares fitting gives the following expression for a horizontal tune shift (x in cm):

$$1000 \cdot \Delta v_x = -0.8 + 3x + 10x^2 + 0.84x^3 + \cdots.$$

From the other hand, the gradient error $\delta k = \delta B_1/B\rho$, where $B_1 = \text{d}B_z/\text{d}x$, produces a horizontal tune shift according to

$$\Delta v_x = \frac{1}{4\pi}\int \beta_x(s)\delta k(s)\,\text{d}s,$$

and the gradient error itself can be represented as a series

$$\delta B_1 = \delta B_{10} + B_2 x + \tfrac{1}{2}B_3 x^2 + \tfrac{1}{6}B_4 x^3 + \cdots,$$
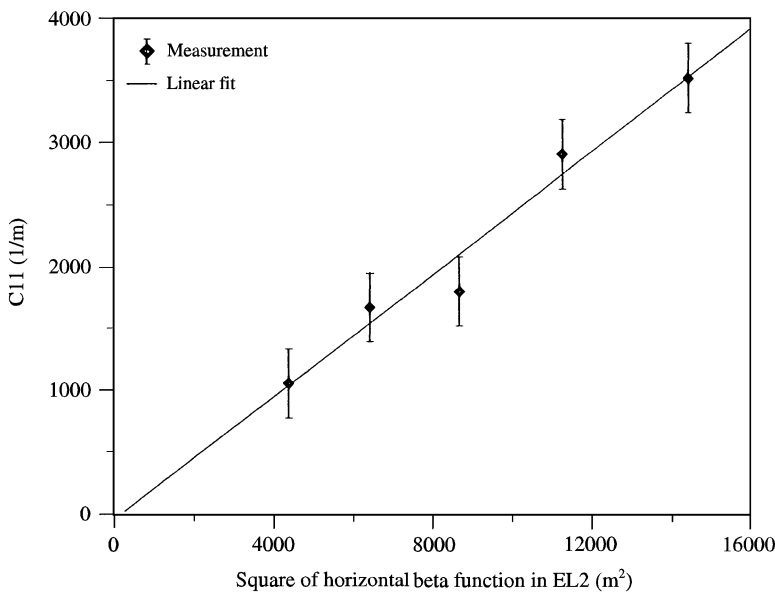
$$B_n = \frac{\text{d}^n B_z}{\text{d}x^n}.$$

Fig. 3. Dependence of the C_{11} coefficient on the β_x^2 value in the FF quadrupoles.
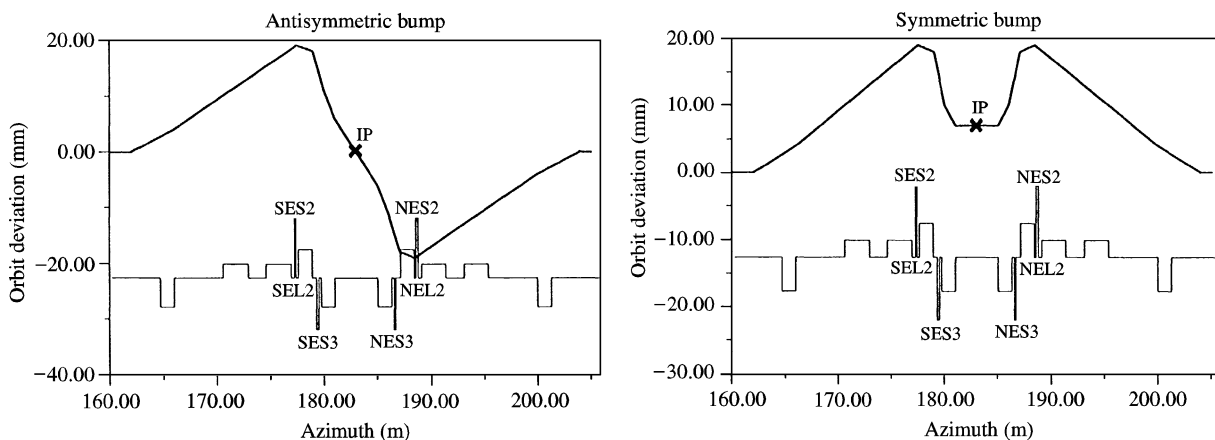

Fig. 4. Closed-orbit bump to measure the integrated magnetic field distribution by electron beam around the interaction point (IP). Left – antisymmetric, right – symmetric.

Comparison with the measurement results gives us the octupole error in the FF quadrupole $O \simeq 0.5 \, \text{G/cm}^3$ that agrees well with the previous estimation.

3. Due to the symmetry of the vector magnetic potential, a dodecapole componet B_5 is an inherency of a quadrupole field. For an ideal

quadrupole magnetic field is represented as

$$B_z = B_1 x + \tfrac{1}{5!} B_5 x^5 + \cdots.$$

Hence, the octupole component in a quadrupole lens is proportional to the dodecapole and squared closed-orbit distortion $O \propto B_5 x_{\text{co}}^2$. To check it, we made a symmetric local bump in the
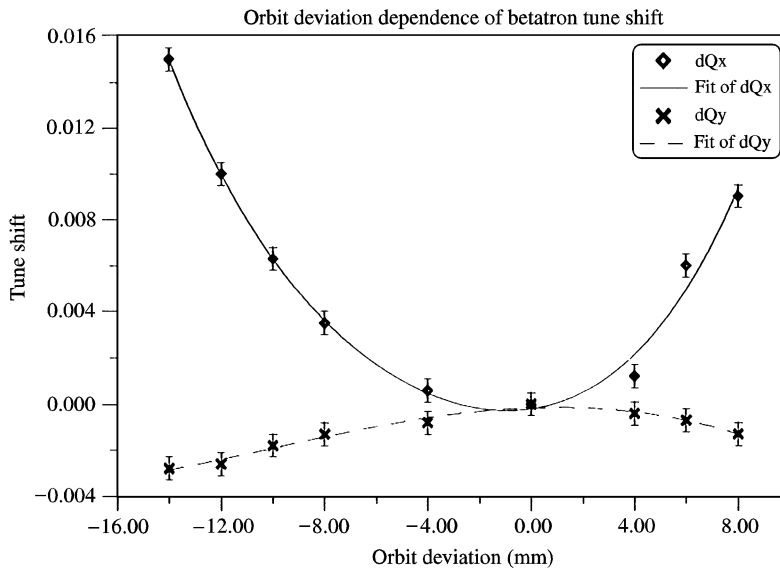
Fig. 5. Betatron tune shift as a function of orbit deviation in the FF quadrupoles in case of the antisymmetric bump.
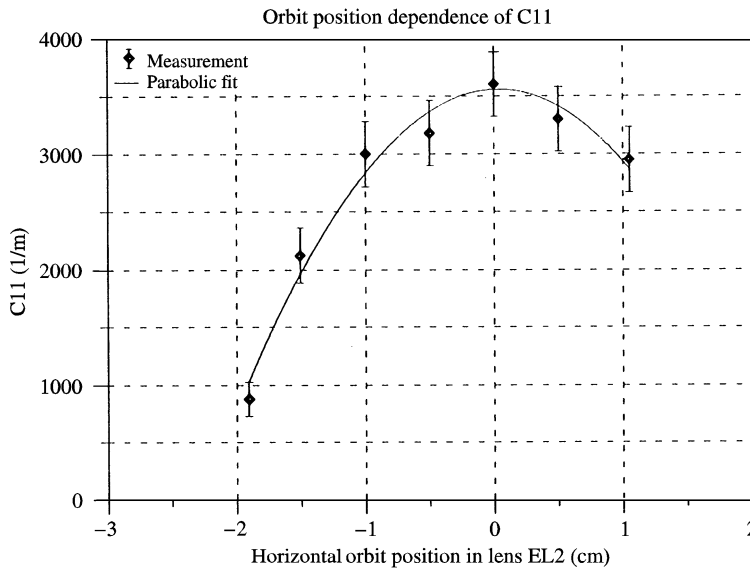

Fig. 6. C_{11} coefficient as a function of the COD in the FF quadrupoles.

FF region and study the horizontal amplitude-dependent tune shift as a function of x_{co}. The result is depicted in Fig. 6. Estimation of the dodecapole value gives

$$B_5 \simeq 0.2 \frac{G}{cm^{-5}} \simeq 2.4 \times 10^4 \, m^{-6}.$$

These measurements seem to point out the FF quadrupoles as a probable source of strong horizontal detuning due to octupole field error $O \simeq 0.5 \, G/cm^3$ (1.8 GeV). Unfortunately, direct field measurement gives only half of this value and the reason for this discrepancy was not understood yet.

4. Phase space trajectories

The method of plotting phase space trajectories in a real machine, similar to computer tracking, was proposed at SPEAR [13,14] and is now widely used in many accelerator laboratories. Two BPMs, spaced in betatron phase by $\pi/2$, provide a turn-by-turn signal, from which one can reconstruct a phase space structure at a single-phase plane.

At VEPP-4M we have such pair of BPMs equipped with turn-by-turn electronics. To study phase space topology, we tracked motion of a beam centroid with a usual two BPMs technique and with a single BPM station. As it will be shown below, the later, in some sense, can be more convenient than two BPMs.

Let us consider a horizontal betatron oscillation tracked by a BPM:

$$x(n) = a\beta_x^{1/2} \cos 2\pi n v_x,$$

$$x'(n) = -a/\beta_x^{1/2}[\alpha_x \cos 2\pi n v_x + \sin 2\pi n v_x], \qquad (3)$$

where $\alpha_x = -\beta'_x(s)/2$ and $\beta_x(s)$ are betatron functions, and a phase advance for nth turn equals $2\pi n v_x$. This expression can be rewritten in the form

$$x'(n) = [x_{\pi/2}(n) - \alpha_x x(n)]/\beta_x,$$

where $x_{\pi/2}(n)$ can be regarded as a coordinate measured by the BPM for which (i) α_x, β_x are equal to those for the first BPM, (ii) the phase advance is exactly $\pi/2$. Introducing "angle-action" variables (J_x, ϕ_x) and substituting Eq. (3) we can obtain

$$J_x(n) = (x_{\pi/2}^2(n) + x^2(n))/2\beta_x,$$

$$\tan \phi_x(n) = x_{\pi/2}(n)/x(n). \qquad (4)$$

One can see that α_x cancels out in the expression for $J_x(\phi_x)$ and phase curves demonstrate "mere" nonlinear distortion.

Usually, a displacement $x(n)$ and a slope $x'(n) \propto x_{\pi/2}(n)$ of a kicked beam are measured by two BPMs at every turn and pictured as a Poincaré map (Fig. 7, top). A nonzero α_x provides an additional distortion of the phase space structure in (x, p_x) that interferes with real nonlinear distortion. To reconstruct the phase curve in "angle-action" variables, we need to know accurately β_x and β'_x at

the position of the BPMs. Although at VEPP-4M beta-functions are measured routinely [15], accurate reading β'_x is not easy. We measured β_x at four pick-up stations adjacent to each of each turn-by-turn BPMs, fit these points to the theoretical curve and extract β_x and β'_x at the azimuth of our BPMs. The resulting plots are shown in the top of Fig. 7.

However, the same map can be pictured more easily using a single BPM approach when the beam displacement and slope are taken from the same turn-by-turn coordinate sequence. For each x_k we select x_{k+n} according to the condition $2\pi\{v_x\}n = (2m + 1)\pi/2 + \delta$, where $\{v_x\}$ is the fractional tune, n, m are integers and δ is the tolerance for the phase shift. For $\delta = 0.02$ in our tune region $n = 2$. Under this approach, α_x, β_x are the same for both values in each pair and expression (4) is valid. It can be shown that the chosen δ gives a relative error in action and angle less than 1%. Additionally, applying FFT and using few main harmonics to construct the beam slope and displacement [16], permits us to reduce drastically the measuring noise and increase the resolution of the phase trajectories distortion. Fig. 7 (bottom) shows a single BPM phase portrait after a reconstruction from an inverse Fourier transform.

From the nominal tune point we can reach a single-degree-of-freedom resonances $3v_x = 26$ and $4v_x = 35$. We explored nonlinear effects of horizontal motion in a vicinity of both the resonances.

4.1. Resonance $3v_x = 26$

Computer tracking shows that the resonance $3v_x = 26$ is driven mainly by the strong chromatic sextupoles in the interaction region. In the vicinity of the resonance $3v_x = m$, we can obtain the phase trajectory $J_x(\phi_x)$ as a solution of the following equation [12]:

$$\bar{J}_x \simeq J_x - f_{3m}J_x^{3/2} \cos 3\phi_x,$$

$$f_{3m} = 6\sqrt{2}\frac{A_{3m}}{3v_x - m},$$

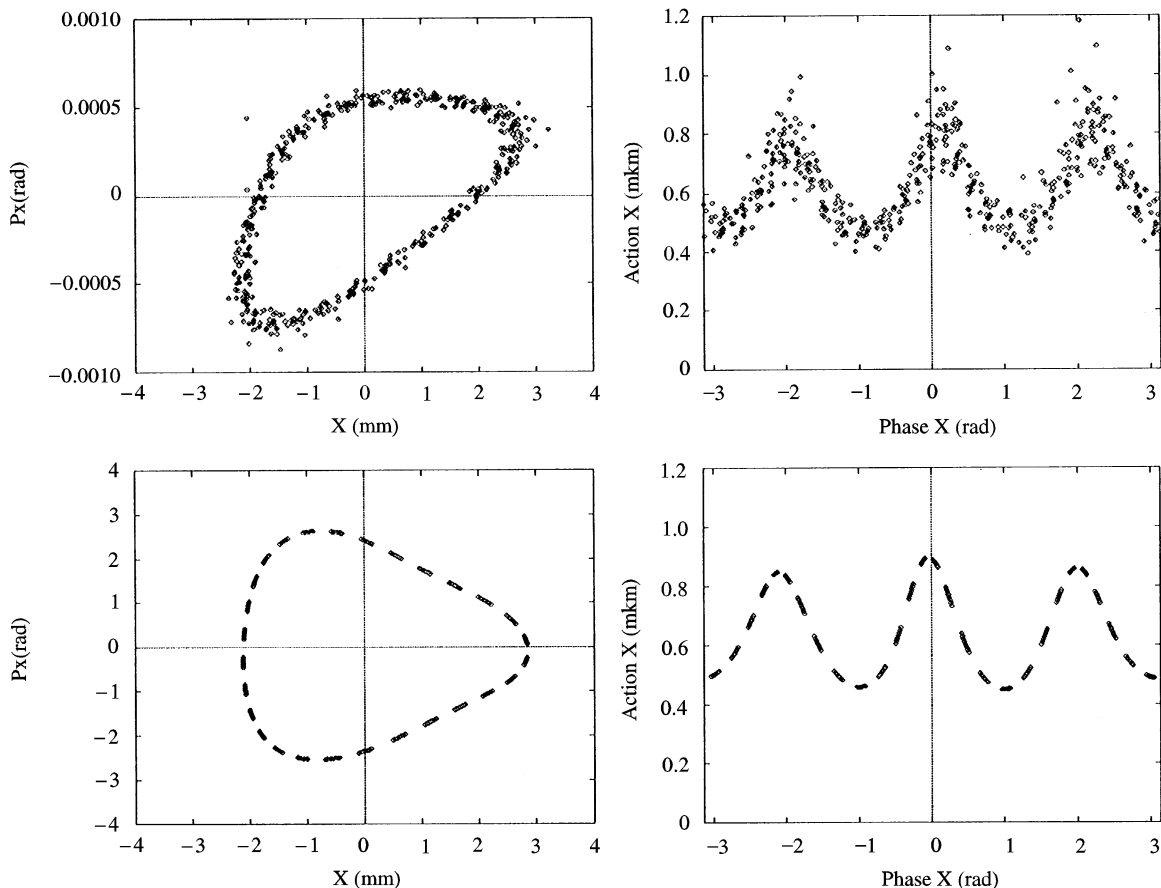where $\bar{J}_x = $ const. can be found from the initial value of the oscillation amplitude, and A_{3m} is an

Fig. 7. Horizontal phase trajectory measured by two BPMs (top) and using single BPM (bottom) ($v_x = 8.69$). Left pictures present trajectories in (x, p_x) variables while right pictures in (J, ϕ) variables.

azimuthal harmonic of the sextupole perturbation

$$A_{3m} =$$

$$\frac{1}{48\pi} \int_0^{2\pi} \beta_x^{3/2}(\theta) S(\theta) \cos\left(3(\psi_x(\theta) - v_x\theta) + m\theta\right) d\theta.$$

Here $S(s) = (d^2 B_z(s)/dx^2)/B\rho$ is normalized sextupole strength.

Fig. 8 shows results of the phase space measurement at $v_x = 8.62$ for different kick amplitudes. The inverse Fourier transform was employed. For this resonance, fixed points are unstable (except for one at the origin) and no stable islands can be seen. Nevertheless, nonlinear motion is easily observed by phase trajectories distortion.

To verify the experimental data, numerical tracking was used in a model of the machine where all known nonlinear effects are included and unknown but predicted in the previous section octupole error is introduced in the FF quadrupoles. The resulting data are plotted in Fig. 8 and demonstrate good agreement with the measured points. Besides, we used a simple Hamiltonian representation to calculate the countur $H = $ const. for the initial experimental conditions. For the largest kick this countur is shown as a solid line in Fig. 8.

Since nonlinear perturbation contributes to phase space distortion at a level of 0.1 mm, for further noise reduction we use for each kick strength data accumulation and averaging. In our
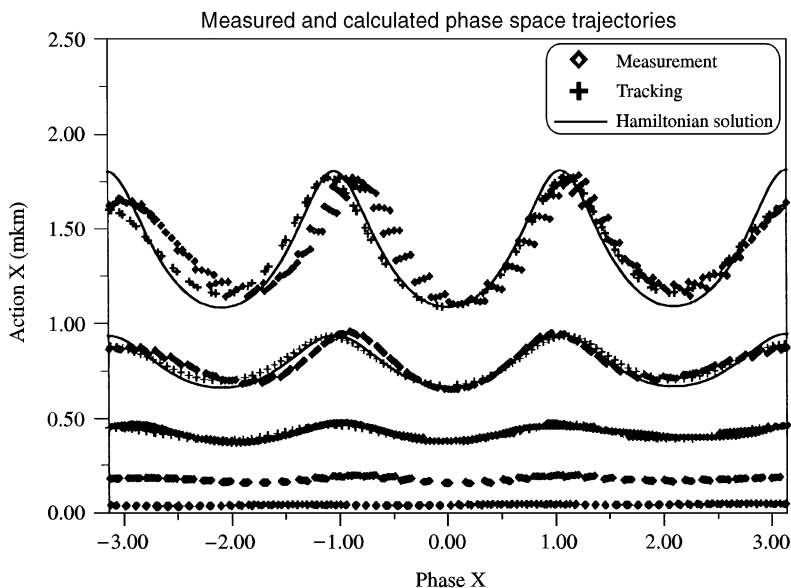
Fig. 8. Measured and calculated phase map ($v_x = 8.62$).

case, a 10 fold accumulation allows to reduce the rms noise value from 10–20 μm to 4–6 μm. Such spectral resolution permits us to calculate some parameters of the nonlinear system. For instance, we can estimate nonlinear perturbation as

$$f_{3m} = \frac{J_{max} - J_{min}}{J_{max}^{3/2} + J_{min}^{3/2}} \simeq \frac{\Delta J}{2\bar{J}^{3/2}},$$

where $\bar{J}$ is the action averaged over the phase angle.

Fig. 9 demonstrates dependence of ΔJ on $\bar{J}^{3/2}$ for different kick amplitudes. One can see that this is a linear dependence and the resonance driving term can be extracted from it. The experimental value is $A_{3\,26} = -2.8 \pm 1.0\,\text{m}^{-1/2}$, while tracking with chromatic sextupoles predicts $A_{3\,26} = -2.1\,\text{m}^{-1/2}$. The agreement seems to be not bad.

To demonstrate the influence of the high beta sextupole SES/NES to beam dynamics we decreased excitation current from 8 to 4.4 A and redistributed chromaticity compensation to the arc sextupole correction coils. A reduction of the phase curve distortion is easily seen in Fig. 10.

4.2. Resonance $4v_x = 35$

Fourth-order resonance was studied in-depth in Ref. [1]. Similar resonance $4v_x = 35$ can be reached from our nominal working point. Fig. 11 shows the phase map in normal coordinates (x, p_x) at the tune $v_x = 8.752$ (left) and $v_x = 8.748$ (right). The first plot demonstrates beam motion near the resonance while the second one shows the particles kicked inside the islands. Processing of the experimental data gives us features of the nonlinear motion and allows us to compare the characteristic of our nonlinear model with those evaluated in the previous sections.

The beam trajectory returns to the same island every fourth revolution. Successive points inside the island should form a closed trajectory around a stable fixed point but in our case the motion inside the island is smeared. The reason, as it was pointed out in Ref. [1], could be either transverse betatron coupling or measurement noise.

The Fourier spectrum under the resonance condition (Fig. 12) detects no linear coupling peak so we made a conclusion that in our case the main reason for the smearing is measurement noise. The
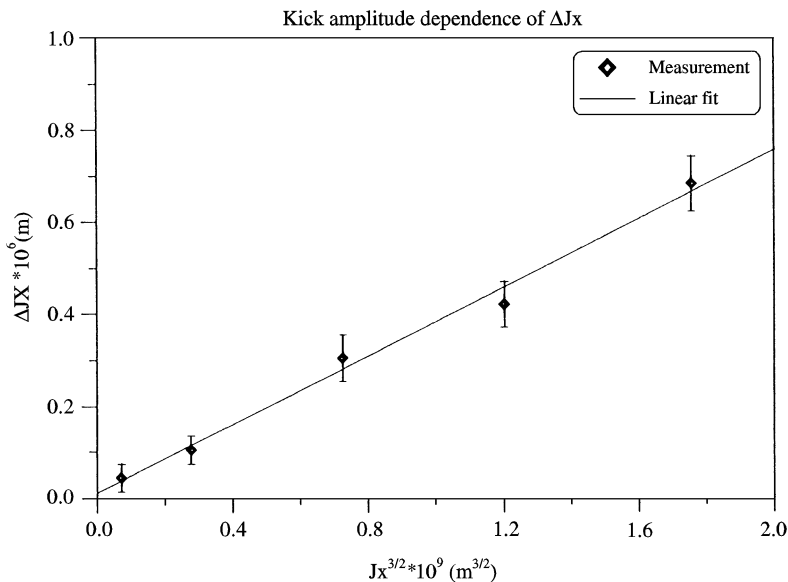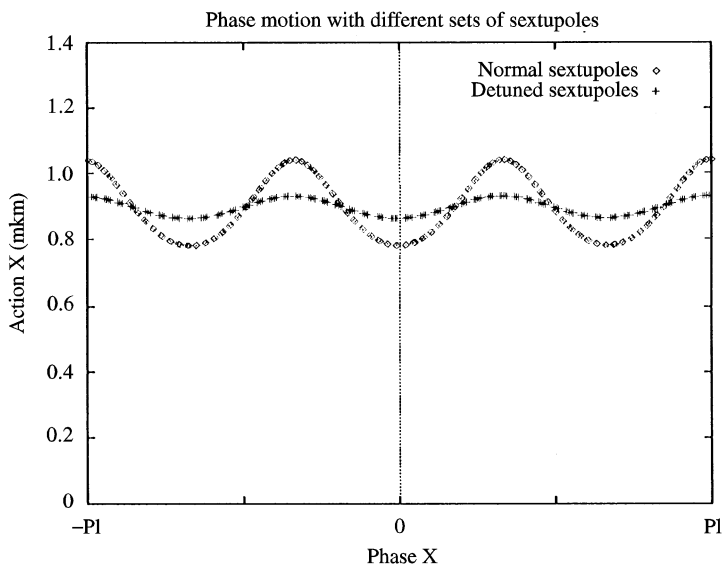
Fig. 9. ΔJ as a function of $\bar{J}^{3/2}$.

Fig. 10. Measured phase curves: usual and reduced sextupoles.

resonance island oscillation is a slow motion and this fact allows us to use the moving averaging which effectively reduces the noise. The resulting stable ellipses are shown in Fig. 13 in (x, p_x) and (J_x, ϕ_x) variables.

The measurement results provide an island tune $\Omega = 0.0013 \pm 0.0001$ that corresponds to a period of 190 ± 15 orbital revolutions.

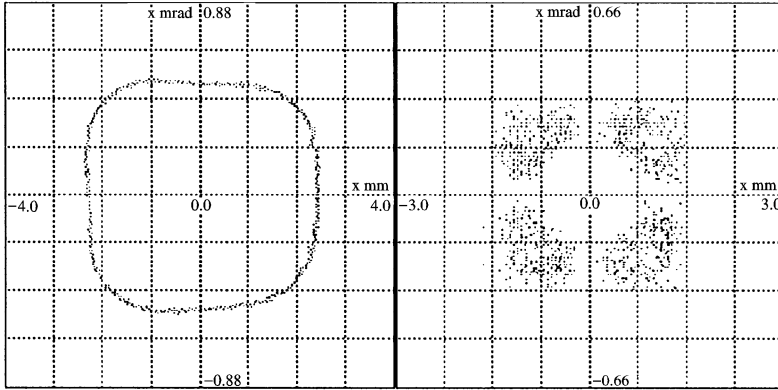To evaluate the parameters of our nonlinear system we used general form of isolated resonance

V. Kiselev et al. /Nucl. Instr. and Meth. in Phys. Res. A 406 (1998) 356–370

367

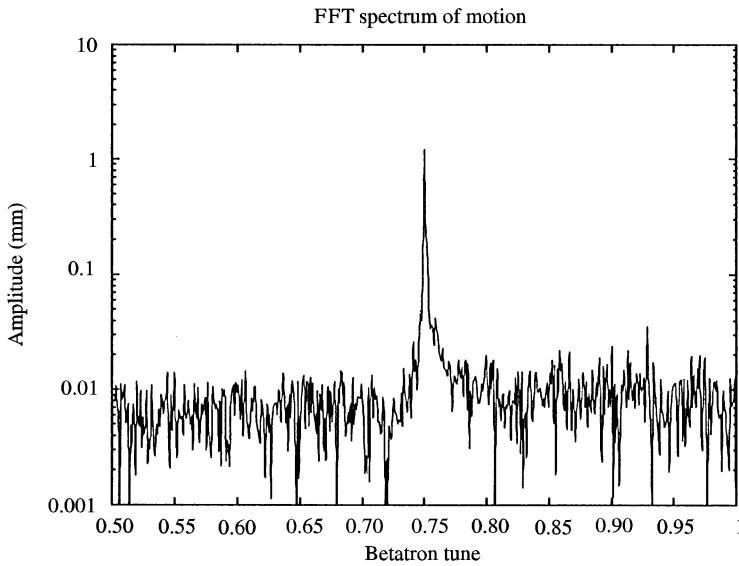Fig. 11. Phase trajectories near and at fourth-order resonance.

Fig. 12. Fourier spectrum of the motion on the resonance $4v_x = 35$.

Hamiltonian, transformed to the rotating system in phase space [20]

$$H_r = \delta I + \alpha(I) + f(I)\cos m\phi. \qquad (5)$$

In our case, when the resonance $4v_x = 35$ is considered ($m = 4$), the distance from the resonance $\delta = v_x - 8.75$, the detuning $\alpha(I)$ relates to the detuning coefficient introduced earlier as $\alpha(I) = C_{11}I^2$ and the resonance driving term corresponds to the relevant azimuthal harmonic as $f(I) = A_{435}$. For small amplitudes the oscillation frequency is given by

$$\Omega^2 = \alpha''(I_r)f(I_r)m^2,$$

where I_r is the amplitude which yields the oscillation frequency at resonance and the prime indicates differentiation with respect to I. The results of fitting the constant Hamiltonian counturs to the
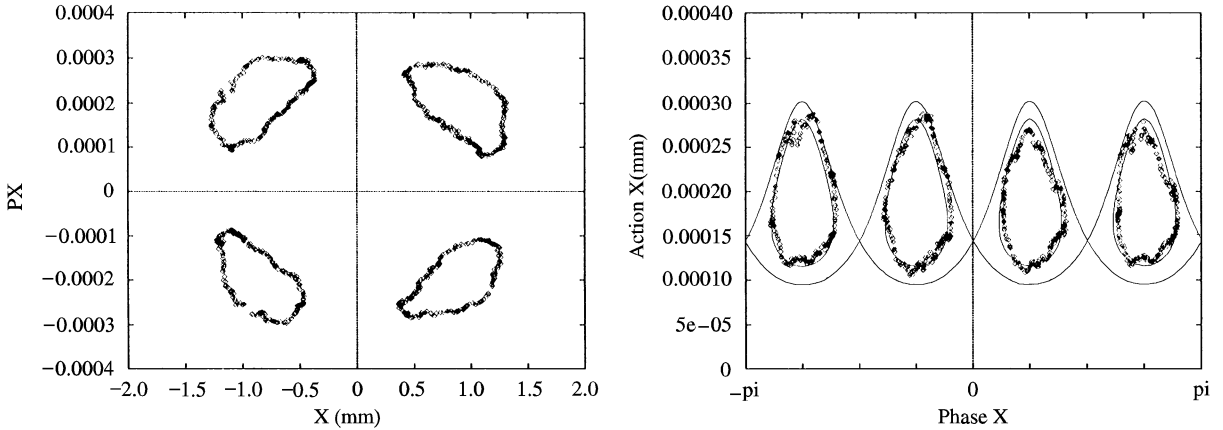
Fig. 13. Motion on resonance $4v_x = 35$.

experimental data plot is shown in Fig. 13 in action-angle coordinates.

The fitting yields the following parameters of the resonance Hamiltonian:

$$\Omega = 0.0013 \pm 0.0001,$$

$$C_{11} = 3600 \pm 200 \, \text{m}^{-1},$$

$$I_r = 1.7 \times 10^{-7} \, \text{m},$$

$$A_{435} = 550 \pm 50 \, \text{m}^{-2}.$$

Supposing, as previously that the main octupole error concentrates in the FF quadrupoles, the value of the error needed to produce the measured harmonic A_{435} is deduced to be about $O \simeq 0.6 \, \text{G/cm}^3$. One can see that the parameters obtained from the fourth-order resonance are in good agreement with those extracted from the experiments described above.

5. Beam distribution

To visualize the beam profile, dissector tubes are used at VEPP-4M [18]. The dissector is a scanning photoelectron device providing information about electron distribution and beam size in transverse

and longitudinal directions. A pulse of radiation from the electron beam produces at the photocathode an image reproducing time structure of the light pulse. Scanning of the image provides an anode signal of the secondary electron multiplier tube that repeats the shape of the observed distribution. In stroboscopic mode the dissector provides time resolution of 2 ps.

Fig. 14 (left) demonstrates the horizontal beam profile at the normal conditions ($v_x = 8.62$). The beam size is much smaller than the dynamic aperture and no distortion of phase trajectories is detected: the Gaussian shape of the intensity distribution with $\sigma_x = 0.6$ mm is determined by quantum fluctuation. To enhance the nonlinearity, we shifted the horizontal tune to the sextupole resonance $3v_x = 26$. In Fig. 14 (right) a typical triangular beam profile is shown at $v_x = 8.6709$ (cf. Ref. [19], where the wire scanning measurements of the beam distribution are described). At the same time, the beam lifetime approaches about 40 s that corresponds to an aperture limitation of about $4.5\sigma_x$. When the excitation of the SES/NES sextupoles was decreased in a factor of two, the same profile was obtained at $v_x = 8.6703$, i.e. much closer to the third-order resonance.

Hamiltonian (5) represents the third-order resonance $3v_x = m$, but with different coefficients

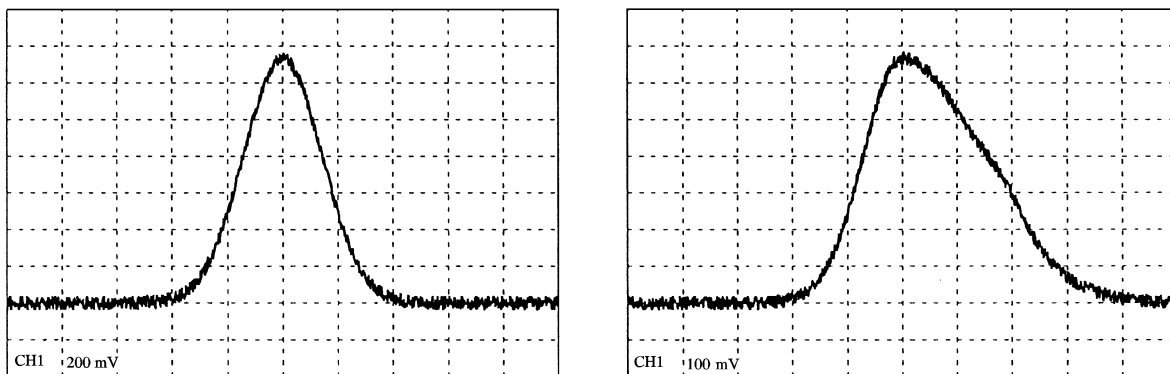$$H_r = \delta_3 I_x + C_{11} I_x^2 + f_3 I_x^{3/2} \cos 3\phi_x,$$

Fig. 14. Electron beam profiles measured with the dissector tube (Left) normal conditions (right) close to resonance $3v_x = 26$.

where $\delta_3 = v_x - m/3$, $f_3 = 2\sqrt{2}A_{3m}$ and A_{3m} is the azimuthal sextupole harmonic. The boundary of the stable area is formed by curves joining unstable fixed points which can be found by the conditions

$$\frac{\partial H_r}{\partial I_x} = \frac{\partial H_r}{\partial \phi_x} = 0,$$

which yields ($\delta_3 < 0$, $C_{11} > 0$)

$$I_{fp}^{1/2} = \frac{3f_3}{8C_{11}}\left(\sqrt{1 + \frac{32}{9}\frac{\delta_3 C_{11}}{f_3^2}} - 1\right). \tag{6}$$

The beam lifetime of 40 s requires the aperture size of $4.5\sigma_x$ (in our case the horizontal damping time is equal to 30 ms). Substituting this value in Eq. (6), we evaluate the magnitude of the sextupole harmonic $A_{326} = -2.7\,\mathrm{m}^{-1/2}$ that nicely agrees with that obtained from the phase space distortion.

6. Conclusion

We studied two aspects of nonlinear dynamics, namely, amplitude-dependent tune shift and phase space trajectories, at the VEPP-4M electron–positron collider. The measurements were performed by the single turn-by-turn BPM technique and by the dissector tube. The experiments indicate that the features of our nonlinear system are strongly influenced by octupole perturbation that does not

follow from the model lattice representation. All measurement results agree well with the theoretical prediction if we assume small (about $0.5\,\mathrm{G/cm^2}$) octupole error in the final focus quadrupoles. Unfortunately, direct magnetic measurement provides only one-half of the required value. This discrepancy is a topic for further investigation.

References

[1] S.Y. Lee et al., Phys. Rev. Lett. 67 (27) (1991) 3768.
[2] J.Y. Liu et al., Phys. Rev. E 49 (1994) 2347.
[3] A. Chao et al., Phys. Rev. Lett. 61 (1988) 2752.
[4] S.G. Peggs, CERN 88-04, 1988, pp. 95–144.
[5] J. Bridges et al., Part. Accel. 28 (1990) 1.
[6] J. Liu et al., Part. Accel. 41 (1993) 1.
[7] S. Kamada et al., Part. Accel. 27 (1990) 221.
[8] J. Gareyte, Part. Accel. 27 (1990) 187.
[9] W. Fischer, M. Giovannozzi, F. Schmidt, The dynamic aperture experiment at the CERN SPS, CERN SL/95-96, AP, 1995.
[10] V. Kiselev, E. Levichev, V. Sajaev, V. Smaluk, Dynamic aperture measurement at the VEPP-4M storage ring, Part. Accel., in press.
[11] R.A. Bech, R. Belbeoch G. Gendreau, Shifts in betatron frequencies due to energy spread, betatron amplitudes and closed orbit excursions. Proc. Conf. HEAC'67, Cambridge A63, 1967.
[12] E. Forest et al., Sources of amplitude-dependent tune shift in the PEP-II design and their compensation with octupoles. Proc. EPAC'94, London, vol. 2, 1994, pp. 1033–1035.
[13] P.L. Morton et al., A diagnostic for dynamic aperture. SLAC-PUB-3627.

[14] J. Bridges et al., Part. Accel. 28 (1990) 1.

[15] A.S. Kalinin et al., Beam diagnostic system for storage rings, Proc. EPAC'96, vol. 2 p. 1582.

[16] P. Krejcik, Dynamic aperture and invariance behaviour in the CERN Antiproton Collector, CERN 88-04, 1988, 145.

[17] E. Levichev, V. Sajaev. AIP Conf. Proc. 344, 1995, pp. 160–169.

[18] E.I. Zinin, Nucl. Instr. and Meth. 208 (1983) 439.

[19] L. Evans et al., The non linear dynamic aperture experiment in the SPS, Proc. EPAC'88, p. 619.

[20] R.D. Ruth, Single particle dynamics and nonlinear resonances in circular accelerators, SLAC-PUB-3836, November 1985.

[21] K.G. Steffen, High Energy Beam Optics, Interscience publishers, New york, 1965.